2025 International Conference on Intelligent Computing
July 26-29, Ningbo, China
https://www.ic-icc.cn/2025/index.php

Research on Motor Optimization Method for Seeder System Based on IWMA-RBF

Xu Chen[1,2], Qinglong Meng[1,2(✉)], Ruirui Sun[1,2], Xudong Miao[1,2], Fengqi Hao[1,2], Qingyan Ding[1,2], and Jinqiang Bai[1,2]

[1] Key Laboratory of Computing Power Network and Information Security, Ministry of Education, Shandong Computer Science Center (National Supercomputer Center in Jinan), Qilu University of Technology (Shandong Academy of Sciences), Jinan, China
[2] Shandong Provincial Key Laboratory of Industrial Network and Information System Security, Shandong Fundamental Research Center for Computer Science, Jinan, China
mengql@sdas.org

Abstract. To address the issues of nonlinearity and strong coupling characteristics in seeder motor systems, and the insufficient dynamic response and weak anti-disturbance capability of traditional control methods. This study proposes an active disturbance rejection control (ADRC) method based on an improved whale migration algorithm (IWMA) optimized radial basis function (RBF) neural network. First, building upon the whale migration algorithm (WMA), a leader proportion dynamic adjustment mechanism is introduced to optimize the population structure through a nonlinear attenuation function. Second, the global search capability is enhanced by integrating a hybrid guidance strategy and Lévy flight perturbation mechanism, thereby constructing the IWMA algorithm with high-efficiency optimization performance. Third, the IWMA is combined with the RBF neural network to collaboratively optimize the RBF network's center vectors, kernel width, and output weights, forming an IWMA-RBF parameter self-tuning framework. Furthermore, an IWMA-RBF-based ADRC controller is designed. The dynamic compensation capability for disturbances such as sudden soil resistance changes is strengthened through an improved extended state observer (ESO), and multi-objective optimization of nonlinear state error feedback (NLSEF) gain parameters is achieved using the IWMA-RBF algorithm. Simulation experiments demonstrate that compared to traditional PID, ADRC, and RBF-ADRC controllers, the IWMA-RBF-ADRC controller significantly improves control accuracy, response speed, and robustness in the motor control system. Field seeding trials verify the superior stability and response speed of this method in complex seeding environments, providing effective technical support for practical applications.

Keywords: Seeder Motor Control, IWMA, RBF, ADRC, Parameter Self-Tuning

1 Introduction

Seeders, as the core equipment of modern agricultural machinery, has operational precision that directly affects crop seedling emergence rates and yield. With the advancement of precision agriculture technology, the electro-control systems of seeders must achieve centimeter-level spacing control under complex field conditions, imposing higher requirements for motor dynamic response speed, anti-interference capability, and parameter self-adaptation characteristics [1]. However, seeder motor systems exhibit significant nonlinearity and strong coupling characteristics. Combined with random disturbances such as sudden changes in soil resistance and mechanical vibrations, conventional PID control methods often fail to adapt to dynamic conditions due to fixed parameters, leading to frequent issues like overshoot oscillations and anti-disturbance lag[2].

In recent years, Active Disturbance Rejection Control (ADRC) technology has demonstrated significant advantages in the field of electromechanical system control due to its unique disturbance observation and compensation mechanism [3]. However, the parameter tuning of ADRC involves multi-variable coordination optimization including Nonlinear State Error Feedback (NLSEF) gains and Extended State Observer (ESO) bandwidth, where traditional trial-and-error methods struggle to overcome the bottleneck of local optima [4]. The radial basis function (RBF) neural network, leveraging the local approximation characteristics inherent in its three-layer feedforward structure, can precisely describe the dynamic characteristics of controlled objects through nonlinear mapping. The radially symmetric distribution of activation functions in its hidden layer neurons not only possesses nonlinear function approximation capabilities but also exhibits faster convergence speed, providing crucial technical support for real-time control scenarios [5]. The deep integration of RBF neural networks with ADRC can fully exploit the former's nonlinear approximation capability to achieve dynamic tuning advantages for controller parameters [6,7]. But, gradient optimization of its central vectors and kernel width parameters is prone to premature convergence.

To explore better network structures and enhance neural network performance, metaheuristic algorithms have emerged as a reliable alternative. Compared to gradient descent methods, metaheuristic algorithms demonstrate higher efficiency in avoiding local optima by shifting from local to global search, making them more suitable for global optimization. Consequently, researchers have adopted metaheuristic algorithms as optimization strategies for RBF network structures, achieving a series of meaningful results thus far. For example, Yang et al. (2023) proposed the Chaotic Adaptive Whale Optimization Algorithm (CASAWOA) to simultaneously optimize RBF center vectors and kernel width, achieving 97.77% accuracy in power transformer fault diagnosis [8]. Elansari et al. (2023) developed a hybrid kernel RBF network architecture (MRBFNN) that dynamically selects combinations of Gaussian and thin-plate spline kernels via genetic algorithms, significantly improving approximation capabilities in complex functions [9]. Tsoulos et al. (2023) designed a two-stage PSO-GA framework integrating global search with local fine-tuning to enhance high-dimensional parameter optimization efficiency [10]. Zhang et al. (2022) employed a feature compression strategy combined with PSO to optimize RBF input features, substantially reducing state-of-charge

estimation errors in battery packs [11]. Liu et al. (2023) introduced a nonlinear time-varying inertia weight Black Widow Optimization Algorithm for optimizing RBF output weights, enabling high-precision modeling in power load forecasting [12]. Wang et al. (2020) utilized a hybrid particle swarm algorithm to optimize RBF connection weights, enhancing noise resistance and reconstruction quality in medical imaging [13]. Huang et al. (2018) integrated a super-mutated firefly algorithm with RBF networks to create an FPGA-embedded controller for real-time trajectory tracking in intelligent vehicles [14].

Despite the investigation of various metaheuristic algorithms for training RBF networks, local optima still persist. The whale migration algorithm (WMA) is a novel metaheuristic algorithm proposed by Ghasemi et al. in 2025[15], simulates the social collaboration and path optimization processes during humpback whale migration. By employing a leader-follower mechanism and dynamic migration strategies, WMA achieves a balance between global exploration and local exploitation, demonstrating significant advantages in solving high-dimensional nonlinear optimization problems. However, traditional WMA has inherent limitations: fixed leader ratios result in insufficient early-stage exploration efficiency and redundant late-stage exploitation resources; monotonous follower update strategies lead to rigid search paths; and the lack of disturbance escape mechanisms traps populations in local optima.

To address these issues, this study proposes an ADRC control method optimized by an IWMA enhanced RBF neural network. First, a nonlinear decay function dynamically adjusts the leader ratio, combined with a hybrid guidance strategy, to construct the IWMA algorithm with multimodal search capabilities. Second, a unified encoding mapping between RBF network parameters and the optimization space is established, enabling IWMA to collaboratively optimize center vectors, kernel widths, and output weights. Finally, an IWMA-RBF-ADRC controller is designed for seeder motors, enhancing the estimation capability for sudden soil resistance changes through an improved third-order ESO and optimizing multi-objective synergy of NLSEF gain parameters. Simulations and field experiments demonstrate that this method significantly improves control precision and dynamic anti-disturbance performance, providing theoretical foundations and technical support for intelligent control of agricultural electromechanical equipment.

2 A Novel IWMA-RBF Algorithm

2.1 IWMA Algorithm

The WMA is a swarm intelligence optimization algorithm inspired by the migratory behavior of whale groups in nature. This algorithm simulates the social division of labor observed during whale migration, categorizing population individuals into two roles: Leader Whales and Follower Whales, which undertake global exploration and local exploitation tasks, respectively. During initialization, a population of N whales is randomly generated within the search space bounded by the lower limit L and upper limit U. The whales are then sorted based on their fitness values. The top NL individuals with

optimal fitness values are designated as Leader Whales, while the remaining act as Follower Whales. Their position update equations are defined as follows:

$$W_{l_{new}}^{i} = W_{l}^{i} + r_1 \otimes L + r_1 \otimes r_2 \otimes (U - L), i = 1, \cdots, NL. \tag{1}$$

$$W_{f_{new}}^{i} = W_{mean} + rand(1, D) \otimes (W_{f}^{i-1} - W_{f}^{i}) + rand(1, D) \otimes (W_{best} - W_{mean}), \quad i = NL + 1, \cdots, N. \tag{2}$$

Where W_l denotes the leader whale position, W_f denotes the follower whale position, D is the problem dimension, W_{mean} is the current average position of all leader whales, W_{best} denotes the optimal whale position. r_1 and r_2 are the vectors of random numbers from the interval [0,1] with the dimension D, and $\otimes$ is the Hadamard product.

At the end of each iteration, the migratory whale individuals are sorted from best to worst. The positions of whales are updated according to the position update formula and fitness values, and the top NL individuals are re-selected as Leader Whales. However, the WMA algorithm adopts a fixed 50% proportion of Leader Whales, leading to insufficient guidance capacity of high-quality individuals in the early iterations that hinders rapid identification of potential regions. In later iterations, redundant Leader Whale quantities result in population diversity degradation and wasteful exploitation resources. The Follower Whales' update mechanism relies solely on individual historical optima, which tends to cause rigid search paths and premature convergence. Furthermore, the absence of an effective escape mechanism causes the entire population to stagnate due to the "groupthink" effect of information transmission when trapped in local optima regions. To address these issues, this paper improves the WMA algorithm through dynamic adjustment of the Leader Whale proportion and a hybrid guidance strategy.

First, the number of Leader Whales NL is dynamically adjusted using a nonlinear decay function. A higher proportion is set initially to enhance global exploration capability, which gradually decreases to 20% as iterations progress, guiding the algorithm's transition from exploration to exploitation phases. Then, a hybrid guidance strategy is introduced into the position update of Follower Whales. The traditional mean-based update formula is refined into a dynamic weight fusion form, which balances swarm information and individual optimal directions, thereby avoiding search rigidity caused by single-path dependencies. Additionally, to address local optima escape, a probabilistically triggered Lévy flight perturbation is incorporated to leverage its long-jump characteristics for breaking local optima traps [16]. The improved equations are:

$$NL = round(N \cdot (0.5 - 0.3 \cdot \frac{t}{T})) \tag{3}$$

$$W_{f_{new}}^{i} = \begin{cases} w \cdot W_{mean} + (1 - w) \cdot W_{best} + \eta \cdot (W_{f}^{i-1} - W_{f}^{i}), a > 0.3 \\ w \cdot W_{mean} + (1 - w) \cdot W_{best} + \eta \cdot (W_{f}^{i-1} - W_{f}^{i}) + \delta (U - L) \dfrac{u}{|v|^{1/\beta}}, a \le 0.3 \end{cases} \tag{4}$$

$$w = 0.7 \cdot (1 - (\frac{t}{T})^2) \tag{5}$$

Where t is the number of iterations, and T represents the maximum number of iterations. w is the dynamic weight coefficient, η is the constant weight coefficient, δ is the Lévy flight step size scaling factor, u and v are random vectors following the standard normal distribution, β is a constant value, and a is a random number between 0 and 1. The improved WMA algorithm is designated as the IWMA algorithm in this study.

2.2 Algorithm Validation Experiment

To evaluate the performance of the IWMA, this study conducts comparative experiments using one representative function from each of the four categories in the CEC2017 benchmark suite (unimodal, multimodal, hybrid, and composition functions) [17]. The compared algorithms include the classic Whale Optimization Algorithm (WOA) [18], Artificial Ecosystem Optimization (AEO) [19], Butterfly Optimization Algorithm (BOA) [20], Particle Swarm Optimization (PSO) [21], and the original WMA. The experiments adopt unified parameter settings: a population size of 30, a maximum of 500 iterations, and a 30-dimensional search space. Fig. 1 illustrates the three-dimensional topological surfaces of the test functions and the comparative convergence curves of the six algorithms on the corresponding functions.

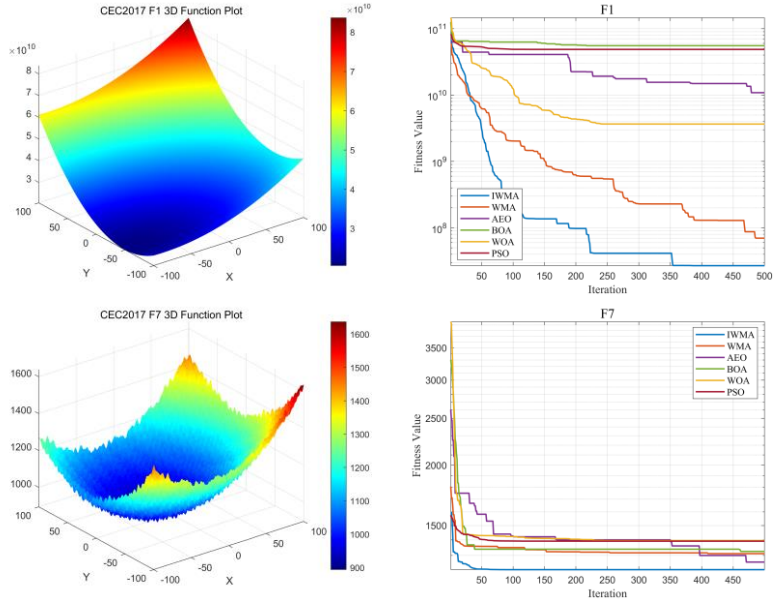

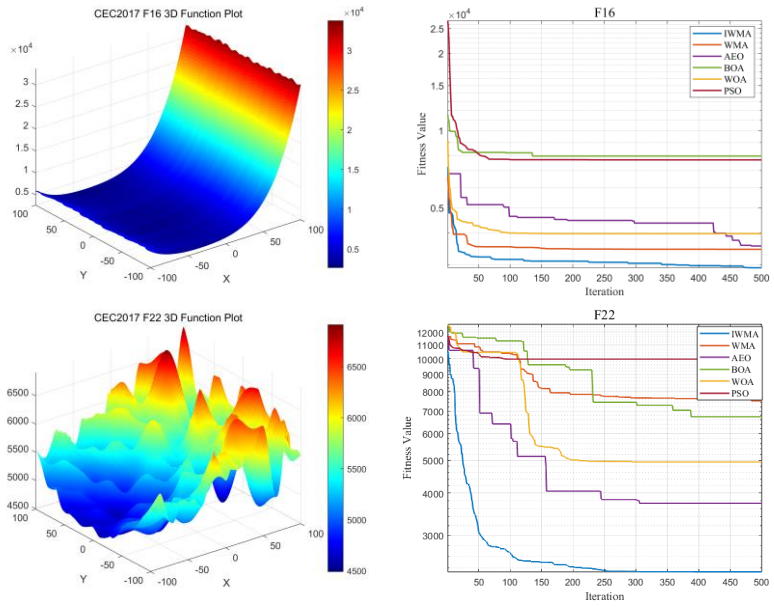

Fig. 1. Presents the convergence curves of the IWMA algorithm and comparison algorithms on different types of test functions in CEC2017.

According to the iterative convergence curves, the IMMA algorithm demonstrates superior performance across various test functions. In the unimodal function F1, IMMA achieves the fastest convergence speed, with its fitness value rapidly decreasing and approaching the optimum within 100 iterations, significantly outperforming other algorithms. For the multimodal function F7, IMMA maintains robust performance in complex multi-extremum environments without noticeable fluctuations throughout the optimization process. In the hybrid function F16, although starting with a relatively high initial fitness value, IMMA rapidly adjusts its strategy and achieves significantly lower fitness values than competitors after 200 iterations. When handling the high-dimensional composite function F22, IMMA exhibits the most pronounced descending trend in fitness values, ultimately reaching the lowest final fitness value with particularly prominent advantages emerging after 300 iterations. While other algorithms (such as BA and GWO) show oscillations or stagnation in later stages, IMMA maintains stable convergence throughout. The improved mechanism of IMMA effectively balances exploration and exploitation capabilities, surpassing other algorithms in convergence speed, precision, and robustness. This enhanced performance makes IMMA particularly suitable for solving multi-modal, highly complex engineering optimization problems.

2.3 IWMA-RBF Algorithm

The RBF neural network is a classic three-layer feedforward supervised learning model, widely used in nonlinear system modeling and pattern recognition due to its rapid convergence capability, local approximation properties, and global convergence advantages. The network consists of an input layer, a hidden layer, and an output layer. The input layer receives raw feature signals and directly transmits them to the hidden layer. The hidden layer performs nonlinear spatial mapping of the input data through radial basis functions (typically Gaussian kernel functions) [22]. The output layer generates final predictions by linearly combining the weighted activation values of the hidden layer nodes. By optimizing the center positions and bandwidth parameters of the hidden layer kernels, as well as the weight coefficients of the output layer, the network efficiently approximates complex nonlinear relationships while avoiding the gradient vanishing problem commonly encountered in traditional backpropagation neural networks.

The Gaussian radial basis function is expressed as:

$$k(x) = \exp\left\{-\frac{\|x-c\|^2}{2\sigma^2}\right\} \tag{6}$$

Where c is the center of the function, and σ is the width (effective range) parameter. When a bias term is incorporated, the output of the RBF neural network can be expressed as:

$$Y(X) = b + \sum_{i=1}^{n} \omega_i \exp(-\frac{(x-c_i)^T (x-c_i)}{2\sigma^2}) \tag{7}$$

Where b is the bias term for output adjustment, w_i represents the connection weights between the hidden layer and the output layer, and n denotes the number of hidden units.

To achieve optimal performance metrics, RBF networks typically employ the k-means clustering algorithm and gradient descent method to calibrate critical parameters (center vectors c, output weights ω, and kernel width σ) [23]. However, these methods suffer from slow convergence and susceptibility to local optima. This paper optimizes these parameters using the IWMA to enhance overall performance. In the IWMA-RBF framework, each whale's position vector encodes the core RBF parameters: the hidden layer centers c (dimensions n × d), Gaussian kernel width σ (dimensions n), and output weights ω (dimensions n), forming a unified optimization space with total dimensionality n×(d+2). Through dynamic leader-whale ratio adjustment, hybrid guidance strategies, and Lévy flight perturbation mechanisms, IWMA enables intelligent exploration of the RBF parameter space.

The procedure of optimizing RBF with the IWMA algorithm is as follows:

1.Encode the parameters to be optimized in the RBF neural network (c, σ, ω) into the solution vector of the optimization problem.

2.Initialize the whale population, where the position vector of each individual is randomly generated.

3.Calculate the fitness value of each individual, update the individual best position and global best position. The fitness function evaluates model performance using cross-validation:

$$F(\theta) = \frac{1}{k}\sum_{i=1}^{k}\left(\frac{1}{n_i}\sum_{j=1}^{n_i}(D_j^i - Y_j^i)^2\right) \tag{8}$$

Where k is the number of cross-validation folds, n_i is the number of samples in the i-th validation set, D_j^i is the expected output value of the j-th sample in the i-th validation set, Y_j^i is the predicted output value of the j-th sample in the i-th validation set.

4.Dynamically select the number of leader whales based on fitness values(Eq.3), then update the position of leading whales according to Eq.1, and update the position of following whales through the hybrid guiding strategy (Eq.4 and 5).

5.Repeat Steps 2-4 until the maximum number of iterations is reached or termination criteria are satisfied.

6.Construct a new RBF neural network using the global best position vector.

3 Controller Design

3.1 ADRC Controller Design

The Tracking Differentiator (TD) achieves smooth approximation of the generalized derivative of the input signal through nonlinear functions in ADRC. It primarily involves two state variables, v_1 and v_2. Here, v_1 represents the state variable tracking the input signal, whose output is the smoothed signal, while v_2 denotes the estimated differential value tracking the input signal, whose output is the differentiated signal [24]. The update equations are:

$$\begin{cases} f = fhan(v_1 - v, v_2, r, h_0) \\ \dot{v}_1 = v_1 + h \cdot v_2 \\ \dot{v}_2 = v_2 + h \cdot f \end{cases} \tag{9}$$

Where v is the input signal, $fhan$ is the fastest control synthesis function for nonlinear optimization tracking, h is the integration step size, r is the speed factor, and h_0 is the filtering factor.

The ESO serves as the core of the ADRC. Traditional third-order ESO compensates for system states in real time through output feedback by estimating unmodeled dynamics, uncertain parameters, and unknown external disturbances, thereby achieving static-error-free control. However, conventional third-order ESO can only estimate current disturbances (e.g., soil resistance, mechanical vibrations) but fails to capture disturbance change trends (e.g., soil resistance mutation rates). In seeder operations, abrupt soil resistance changes may occur at rates of *10–30 N·m/s*, and the lagged compensation from ESO would lead to seeding depth fluctuations, compromising uniformity. To address these limitations and better adapt to seeder systems, a redesigned third-order ESO is proposed, with its core equations expressed as:

$$\begin{cases} e = z_1 - y \\ \dot{z}_1 = z_2 - \beta_{01} \cdot e \\ \dot{z}_2 = z_3 - \beta_{02} \cdot fal(e, \alpha_1, \delta) + bu \\ \dot{z}_3 = -\beta_{03} \cdot fal(e, \alpha_2, \delta) + \gamma \dfrac{dF_{soil}}{dt} \end{cases} \tag{10}$$

Where Z_1 and Z_2 are the observed values of the system states, Z_3 is the total disturbance estimate. y is the actual system output. β_{01}, β_{02}, and β_{03} are the observer gains determining estimation speed and stability; e is the observation error; b is the compensation coefficient. *fal* is the nonlinear function, α_1 and α_2 are the nonlinear factors, and δ is the linear interval threshold. $\dfrac{dF_{soil}}{dt}$ represents the instantaneous rate of change of the soil resistance acting on the seeder opener with respect to time, with units of N·m/s. To obtain this critical information, high-precision force sensors are installed on key force-bearing components of the seeder (such as the opener). This sensor directly and in real-time measures the soil resistance F_{soil} (unit N·m) experienced by the opener, generating corresponding electrical signals. γ is an adjustable gain coefficient used to regulate the contribution weight of the estimated soil resistance change rate in the ESO state update.

$$fal(e, \alpha, \delta) = \begin{cases} \dfrac{e}{\delta^{1-\alpha}}, & |e| \le \delta \\ sign(e) \cdot |e|^{\alpha}, & |e| > \delta \end{cases} \tag{11}$$

The NLSEF acts as the control output module of ADRC. Its core function is to process tracking errors through nonlinear combinations, generating control signals that counteract disturbances and enable precise tracking. Unlike traditional linear PID, NLSEF employs the *fal* function to amplify gain in small-error regions while smoothing responses in large-error regions, thereby adapting to complex nonlinear systems [25]. The structural design of NLSEF is expressed as:

$$\begin{cases} e_1 = v_1 - z_1 \\ e_2 = v_2 - z_2 \\ u_0 = \beta_1 fal(e_1, \alpha_3, \delta) + \beta_2 fal(e_2, \alpha_4, \delta) \\ u = u_0 - \dfrac{z_3}{b} \end{cases} \tag{12}$$

Where u_0 is the control law; β_1 and β_2 are gain parameters; e_1 is the tracking error, e_2 is the error derivative; α_3 and α_4 are the nonlinear factors.

3.2 IWMA-RBF-Based ADRC Controller

Aiming at the nonlinear and strongly coupled control characteristics of the corn planter motor and the high-precision control requirements, this study proposes an intelligent

parameter tuning system integrating ADRC technology with the IWMA-RBF neural network. Within the multi-parameter framework of ADRC, the gain parameters β_1 and β_2 of the NLSEF play dominant roles in determining system dynamics. The disturbance rejection gain β_1 directly governs the system's anti-interference capability and response speed increasing β_1 enhances disturbance suppression and accelerates response, yet requires careful balancing between disturbance rejection and system stability to prevent oscillation caused by excessive parameter values. The dynamic compensation gain β_2 regulates damping characteristics during transitional processes to suppress overshoot, with its optimization significantly improving tracking accuracy and dynamic smoothness. Traditional trial-and-error methods prove inadequate for achieving collaborative optimization of β_1 and β_2, being prone to local optima. To address this, the study innovatively employs the IWMA-RBF algorithm for synergistic parameter optimization, dynamically balancing the constraints between parameters to achieve comprehensive performance enhancement of the controller. The schematic structure of the IWMA-RBF driven ADRC controller is illustrated in Fig. 2.

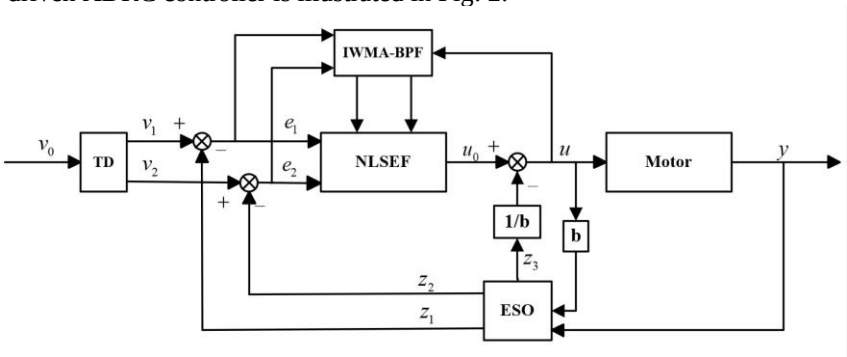

Fig. 2. Structural diagram of the ADRC controller based on IWMA-RBF.

3.3 Simulation Testing and Comparative Analysis

To validate the performance advantages of the IWMA-RBF-optimized ADRC controller in high-precision control of stepper motors, a multi-condition simulation model for the stepper motor was developed on the MATLAB/Simulink platform. Comparative analyses were conducted on the dynamic response characteristics of four controllers PID, conventional ADRC, RBF-ADRC, and IWMA-RBF-ADRC under different operational scenarios. The main parameters of the ADRC controllers are shown in Table 1.

Table 1. Controller Parameters Table

Structure	Parameter	Value
TD	r	5000
	h	0.01
	h_0	0.01
ESO	α_1	0.5
	α_2	0.75

	β_{01}	30
	β_{02}	300
	β_{03}	1000
	δ	0.001
	b	2
	γ	0.15
NLSEF	α_3	0.25
	α_4	0.25

As shown in Fig. 3, In the disturbance-free step response test, the IWMA-RBF-ADRC algorithm demonstrated optimal rapid response and stability. Its response curve reached the target position within approximately 0.1s with zero overshoot throughout the process, indicating the algorithm's strong tracking capability for dynamic systems. In contrast, the PID controller exhibited the slowest rise speed along with approximately 10% overshoot, followed by persistent oscillations near the target position, revealing the limitations of fixed parameters in traditional PID control. Both ADRC and RBF-ADRC eliminated overshoot but required slightly longer convergence times compared to IWMA-RBF-ADRC.

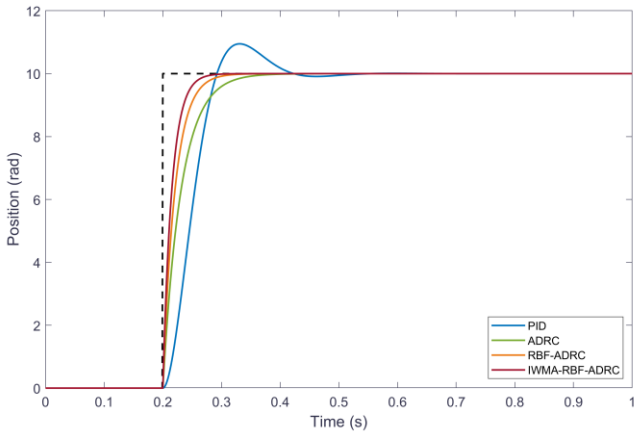

Fig. 3. Response curves of each controller after step signal input.

As shown in Fig. 4, when subjected to a sudden 15 N·m torque load disturbance at 0.5s, all controllers exhibited positional deviations. However, IWMA-RBF-ADRC achieved the fastest recovery speed with minimal position fluctuation amplitude. The PID controller experienced a sharp position drop of approximately 0.5 rad under load disturbance, accompanied by sustained oscillations during recovery, exposing its insufficient disturbance rejection capability.

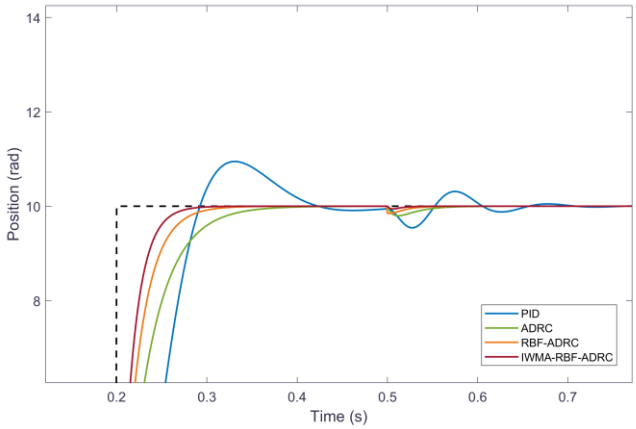

Fig. 4. Response curves of each controller under load.

In the sinusoidal signal tracking test shown in Fig. 5, the tracking curve of IWMA-RBF-ADRC nearly coincides with the target sinusoidal signal without phase lag, indicating that its dynamic response bandwidth fully covers the signal frequency. The other three controllers exhibited noticeable amplitude attenuation and phase lag, further validating that IWMA-RBF-ADRC demonstrates both high-precision tracking capability and strong noise resistance for periodic dynamic signals.

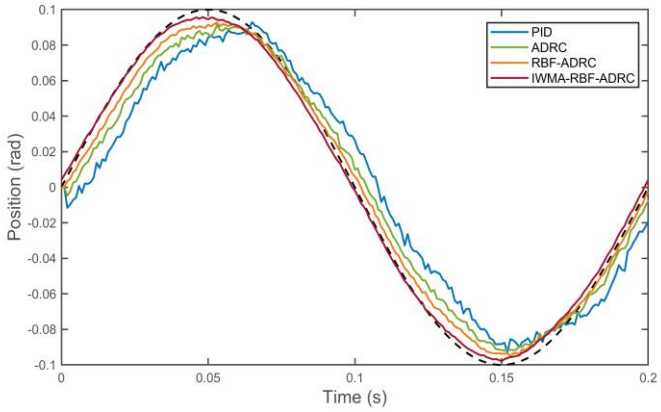

Fig. 5. Response curves of each controller after sinusoidal signal input.

3.4 Seeding Test

To further validate the practical effectiveness of the IWMA-RBF optimized ADRC system in agricultural electromechanical control, field testing was conducted using a constructed experimental platform (see Fig. 6).

Fig. 6. Corn planter experimental platform.

The seeding performance verification experiment was designed as follows: based on the agronomic requirement of a preset 15 cm seed spacing, the real-time rotational speed signal of the tractor's drive wheels was acquired using an incremental encoder, converted to linear velocity by the STM32F407 microcontroller, and dynamically adjusted PWM commands were sent to the stepper motor via CAN bus. To comprehensively evaluate the control algorithm performance, three comparative groups were set: 1. traditional PID controller, 2. classical ADRC controller, 3. IWMA-RBF-optimized ADRC controller. The HMI touchscreen integrated parameter configuration, status monitoring, and anomaly alert functions, enabling real-time display of seeding speed and quantity. During the experiment, the working status of the seeding unit was continuously recorded 10 repeated trials on a 50 m standardized test ridge. The actual seed spacing of 100 consecutive seeding points was manually measured using a high-precision tape (see Fig. 7), and the mean spacing was calculated. The experimental data for the three groups showed: PID control group had an average spacing of 16.5 cm (standard deviation 2.3 cm), maximum deviation ±4.0 cm, and miss-seeding rate of 3.5%; classical ADRC group had an average spacing of 16.1 cm (standard deviation 0.9 cm), maximum deviation ±2.1 cm, and miss-seeding rate of 2.1%; IWMA-RBF-optimized ADRC group had an average spacing of 15.6 cm (standard deviation 0.6 cm), maximum deviation ±1.5 cm, and miss-seeding rate consistently below 1.2% (corresponding to a seeding rate ≥98.8%). When encountering hardened ground interference, the PID control exhibited a persistent 0.8 s speed-tracking lag, resulting in spacing fluctuations of ±2.5 cm, while the IWMA-RBF-optimized ADRC system suppressed fluctuations to within ±1 cm. These results validate that the IWMA-RBF-optimized ADRC system significantly outperforms traditional control methods in spacing accuracy, anti-interference capability, and seeding reliability, meeting the design requirements.

Fig. 7. The red circles in the figure indicate corn seeds sown by the planter. Seed spacing is measured using a ruler.

4 Conclusion

This study addresses the high-precision control requirements of seeder motor systems by proposing an ADRC control method optimized via IWMA-RBF. Through enhancements to the whale migration algorithm, a leader proportion dynamic adjustment mechanism and a hybrid guidance strategy are innovatively introduced, resolving the conflict between insufficient early exploration and redundant late exploitation in traditional WMA. The algorithm demonstrates superior convergence speed and global optimization capabilities in CEC2017 benchmark function tests. By deeply integrating IWMA with the RBF neural network, a collaborative optimization framework with dynamically adaptable parameter encoding dimensions is constructed, effectively overcoming the tendency of traditional gradient descent methods to fall into local optima. The designed IWMA-RBF-ADRC controller employs an improved third-order ESO to predict disturbance variation rates. Combined with multi-objective collaborative optimization of NLSEF gain parameters, the controller exhibits near-zero overshoot and phase-lag-free tracking characteristics in simulations, achieving faster recovery time under sudden 15 N·m load disturbances compared to traditional ADRC. Field trial data further confirm the method's superior seeding accuracy. Future work will extend this approach to multi-motor cooperative operation scenarios and explore real-time parameter adaptive adjustment mechanisms based on edge computing.

Acknowledgments. This study was funded in part by the Research and Development of Soil Multi-Parameter Composite Sensors and Intelligent Monitoring Systems(2024CXGC010905), in part by the Research, Development, and Application of Intelligent Central Air Conditioning and Integrated IoT Configuration Systems for High-End Residential Buildings(2024TSGC0603), in part by the Construction and Application Demonstration of R&D Public Service Platforms for Intelligent Innovation in New-Type R&D Institutions(YDZX2023050), in part by the Intelligent Manufacturing Empowerment Platform Based on Industrial Internet and Its Applications(YDZX2024121), in part by the Research on Key Technologies for Building Trusted Data Spaces and High-Quality Data Elements, and Industry Applications(2024ZDZX08), in part by the Research and Development of Key Sensing Technologies for Growth Factors and Vital Signs

of Greenhouse Crops(2023TSGC0111), in part by the Research on Key Technologies for Intelligent Management and Control of Agricultural Machinery and Information Platforms, and Their Applications(2023TSGC0587).

References

1. Ling, L., Xiao, Y., Huang, X., et al.: Design and Testing of Electric Drive System for Maize Precision Seeder. Agriculture. 14(10), 1778 (2024)
2. Han, J.: From PID to Active Disturbance Rejection Control. IEEE Transactions on Industrial Electronics. 56(3), 900–906 (2009)
3. Liu, L., Liu, Y., Zhou, L., et al.: Cascade ADRC with Neural Network-Based ESO for Hypersonic Vehicle. Journal of the Franklin Institute. 360(12), 9115–9138 (2023)
4. Deng, Y., Zhu, J., Liu, H.: The Improved Particle Swarm Optimization Method: An Efficient Parameter Tuning Method with the Tuning Parameters of a Dual-Motor Active Disturbance Rejection Controller. Sensors. 23(20), 8605 (2023)
5. Fritzke, B.: Fast Learning with Incremental RBF Networks. Neural Processing Letters. 1, 2–5 (1994)
6. Feng, H., Song, Q., Ma, S., et al.: A New Adaptive Sliding Mode Controller Based on the RBF Neural Network for an Electro-Hydraulic Servo System. ISA Transactions. 129, 472–484 (2022)
7. Liu, S., Ding, H., Wang, Z., et al.: An ADRC Parameters Self-Tuning Control Strategy of Tension System Based on RBF Neural Network. Journal of Renewable Materials. 11(4), 1991 (2023)
8. Yang, P., Wang, T., Yang, H., et al.: The Performance of Electronic Current Transformer Fault Diagnosis Model: Using an Improved Whale Optimization Algorithm and RBF Neural Network. Electronics. 12(4), 1066 (2023)
9. Elansari, T., Ouanan, M., Bourray, H.: Mixed Radial Basis Function Neural Network Training Using Genetic Algorithm. Neural Processing Letters. 55(8), 10569–10587 (2023)
10. Tsoulos, I.G., Charilogis, V.: Locating the Parameters of RBF Networks Using a Hybrid Particle Swarm Optimization Method. Algorithms. 16(2), 71 (2023)
11. Zhang, G., Xia, B., Wang, J., et al.: Intelligent State of Charge Estimation of Battery Pack Based on Particle Swarm Optimization Algorithm Improved Radical Basis Function Neural Network. Journal of Energy Storage. 50, 104211 (2022)
12. Liu, H., Zhou, G., Zhou, Y., et al.: An RBF Neural Network Based on Improved Black Widow Optimization Algorithm for Classification and Regression Problems. Frontiers in Neuroinformatics. 16, 1103295 (2023)
13. Wang, H., Liu, K., Wu, Y., et al.: Image Reconstruction for Electrical Impedance Tomography Using Radial Basis Function Neural Network Based on Hybrid Particle Swarm Optimization Algorithm. IEEE Sensors Journal. 21(2), 1926–1934 (2020)
14. Huang, H.C., Lin, S.K.: A Hybrid Metaheuristic Embedded System for Intelligent Vehicles Using Hypermutated Firefly Algorithm Optimized Radial Basis Function Neural Network. IEEE Transactions on Industrial Informatics. 15(2), 1062–1069 (2018)
15. Ghasemi, M., Deriche, M., Trojovský, P., et al.: An Efficient Bio-Inspired Algorithm Based on Humpback Whale Migration for Constrained Engineering Optimization. Results in Engineering. 104215 (2025)
16. Li, J., An, Q., Lei, H., et al.: Survey of Lévy Flight-Based Metaheuristics for Optimization. Mathematics. 10(15), 2785 (2022)

17. Wu, G., Mallipeddi, R., Suganthan, P.N.: Problem Definitions and Evaluation Criteria for the CEC 2017 Competition on Constrained Real-Parameter Optimization. National University of Defense Technology. (2017)
18. Mirjalili, S., Lewis, A.: The Whale Optimization Algorithm. Advances in Engineering Software. 95, 51–67 (2016)
19. Zhao, W., Wang, L., Zhang, Z.: Artificial Ecosystem-Based Optimization: A Novel Nature-Inspired Meta-Heuristic Algorithm. Neural Computing and Applications. 32, 9383–9425 (2020)
20. Arora, S., Singh, S.: Butterfly Optimization Algorithm: A Novel Approach for Global Optimization. Soft Computing. 23, 715–734 (2019)
21. Kennedy, J., Eberhart, R.: Particle Swarm Optimization. Proceedings of ICNN'95 - International Conference on Neural Networks. 4, 1942–1948 (1995)
22. Fornberg, B., Lehto, E., Powell, C.: Stable Calculation of Gaussian-Based RBF-FD Stencils. Computers & Mathematics with Applications. 65(4), 627–637 (2013)
23. Fasshauer, G.E., Zhang, J.G.: On Choosing "Optimal" Shape Parameters for RBF Approximation. Numerical Algorithms. 45, 345–368 (2007)
24. Zhong, S., Huang, Y., Chen, S., et al.: A Novel ADRC-Based Design for a Kind of Flexible Aerocraft. Control Theory and Technology. 19, 35–48 (2021)
25. Yang, X., Huang, Q., Jing, S., et al.: Servo System Control of SATCOM on the Move Based on Improved ADRC Controller. Energy Reports. 8, 1062–1070 (2022)